LANGMUIR

Article

pubs.acs.org/Langmuir

Molecular Thermodynamic Modeling of Reverse Micelles and Water-in-Oil Microemulsions

Boris Lukanov[†] and Abbas Firoozabadi*[,†,‡]

[†]Reservoir Engineering Research Institute, 595 Lytton Avenue, Palo Alto, California 94301, United States

[‡]Department of Chemical Engineering, Yale University, New Haven, Connecticut 06511, United States

Supporting Information

ABSTRACT: Surfactant aggregation plays an important role in a variety of chemical and biological nanoscale processes. On a larger scale, using small amounts of amphiphiles compared to large volumes of bulk-phase modifiers can improve the efficiency and reduce the environmental impact of many chemical and industrial processes. To model ternary mixtures of polar, nonpolar, and amphiphilic molecules, we develop a molecular thermodynamic theory for polydisperse water-in-oil (W/O) droplet-type microemulsions and reverse micelles based on global minimization of the Gibbs free energy of the system. The incorporation of size polydispersity into the theoretical formulation has a significant effect on the Gibbs free energy landscape and allows us to accurately predict micelle size distributions and micelle size variation with composition. Results are presented for two sample ionic surfactant/water/oil systems and compared with experimental data. By predicting the structural and compositional characteristics of w/o microemulsions, the molecular thermodynamic approach provides an important bridge between the modeling of ternary systems at the molecular and the macroscopic level.

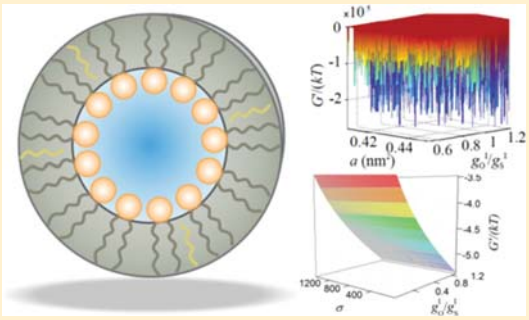

I. INTRODUCTION

Reverse micelles are nanoscale particles composed of surfactant molecules that assemble around an aqueous core suspended in a nonpolar solvent. Similarly, water-in-oil (W/O) microemulsions are dispersions of nanometer-size water droplets in oil, stabilized by the presence of an amphiphilic species at the interface between the two media. The term "oil" can be used very liberally to refer to any nonpolar water-insoluble liquid. These systems have attracted a great deal of attention as they span an impressively wide gamut of practical applications: from the production of lubricants, cleaners, and cosmetics[1] to the synthesis of nanoparticles[2,3] and the development of advanced drug-delivery[4,5] and enhanced oil-recovery methods.[6] They also play an important role in biological systems and have been used to investigate the biophysical properties of encapsulated proteins and DNA, as well as the effects of confinement on protein and water dynamics.[7−11] Understanding the composition, size, and morphology of these nanostructures is of critical importance to many of the applications mentioned above.

In principle, there is no clear distinction between reverse micellar systems and W/O microemulsions. Microemulsions are often considered as large-scale versions of reverse micelles, and terms such as "micellar emulsions" or "swollen micelles" have been used in the literature.[12,13] Both systems, however, contain aggregates in the 5−100 nm size range (larger droplets are usually classified as ordinary emulsions, which, unlike microemulsions, are nonisotropic and thermodynamically unstable). Moreover, it has been shown that reverse micelles always contain an aqueous core and cannot form without trace amounts of water in the nonpolar solvent.[14,15] Thus, the distinction between the two systems may simply be a question of semantics, where the term "reverse micelle" may refer to the nanoparticles themselves, while the term "microemulsion" may denote the entire system containing both the continuous oil phase and the dispersed water phase within the nanoparticle aggregates. In this paper, we employ the terms "reverse micelle", "nanoparticle", "droplet", and "aggregate" interchangeably, whereas the term "microemulsion" will refer to the entire system.

The structure and phase behavior of ternary mixtures of water, oil, and amphiphiles can be very complex, and few theoretical studies have attempted to develop predictive models for such systems. The first efforts examined microemulsions through a macroscopic thermodynamics point of view with the free energy formulated from the known or estimated interfacial tension and the bending free energy of the surfactant monolayer.[16−21] The main limitation of this approach is the requirement for adjustable parameters obtained from experimental regression, and the inability to provide detailed information about both the global phase behavior and the microscopic molecular properties of the system.

A molecular thermodynamic model was first developed by Nagarajan and Ruckenstein.[22] The authors considered the surfactant molecular structure and used equality of chemical

Received: January 11, 2016
Revised: February 23, 2016
Published: February 26, 2016

 © 2016 American Chemical Society

DOI: 10.1021/acs.langmuir.6b00100
Langmuir 2016, 32, 3100−3109

potentials to predict the equilibrium state of the system by varying the amount of surfactant in the mixture. They did not investigate droplet size variation with composition and, to the best of our knowledge, did not compare their results with experimental data. The only other molecular thermodynamic model that we are aware of is by Moreira and Firoozabadi.[23] They adopted parts of Nagarajan and Ruckenstein's theory to develop a theoretical framework for droplet-type microemulsions based on global minimization of the Gibbs free energy. One of the main conclusions in their paper was that the assumption of monodispersity (also known as the maximum term approximation) exploited by both models is not a good approximation and that polydispersity needs to be accounted for, in contrast to micelle formation in aqueous systems.[24] Reverse micelle systems have also been studied using molecular dynamics (MD) simulations.[25−27] MD simulations, however, are computationally expensive and are generally limited to the realm of small-sized systems of one to several droplets only. While they can reveal important details about micelle molecular structure and composition, they cannot currently provide reliable information on the macroscopic properties of the system such as phase behavior or droplet size distribution as a function of overall composition.

In this paper, we develop a molecular thermodynamic theory for polydisperse reverse micelles and W/O microemulsions. One of our goals is to provide a general framework that allows for the prediction of the nanoparticle size distribution and the phase behavior of the system based on global minimization of the Gibbs free energy. Using equality of chemical potentials instead may not provide accurate results, as it may reveal a state of metastable equilibrium, i.e., a system trapped in a local minimum of an often rugged Gibbs free energy landscape. We derive an expression for the total Gibbs free energy, which we then minimize for a system of a given composition, temperature, and pressure with respect to geometrically and compositionally independent variables without adjustable or fitted parameters. The expression for the Gibbs free energy is used together with the free energy of aggregation, which accounts for various contributions related to the formation of the droplet interfacial layer as well as to the surfactant molecular structure, similar to our approach to micellization in water.[24] We include an excess phase in our derivations so that the formulation accounts for both single-phase and two-phase systems, as determined by the Gibbs free energy minimization. We show that the model can accurately predict droplet sizes and size distributions for a range of system compositions.

II. THEORY

A. Geometric and Structural Considerations. Reverse micelles in W/O microemulsions contain an aqueous core region of radius R_W surrounded by an interfacial layer of thickness $R_O - R_W$, as shown schematically in Figure 1. The interfacial layer is hydrophobic in character and contains the hydrophobic tails of the surfactant molecules plus oil molecules incorporated into the interfacial film.

The surfactant hydrophilic heads and adsorbed counterions are located at the surface of charge defined by R_{ch}, i.e., they are physically outside of the interfacial layer but contribute to its energy of formation. The rest of the droplet is occupied by the core region which contains the dispersed water phase. A micelle contains g_j molecules of each component j, where the subscript j = O, W, S denotes the molecule type (oil, water, surfactant). The total number of molecules of each component in the droplet can be further subdivided into those in the interfacial layer and those in the droplet core: $g_j = g_j^I + g_j^{core}$. We assume that there are no surfactant molecules dissolved in the aqueous cores ($g_S^{core} = 0$) and that oil molecules can penetrate only as far as the interfacial region ($g_O^{core} = 0$). We also assume that the interfacial layer is hydrophobic in nature and contains no water molecules ($g_W^I = 0$).

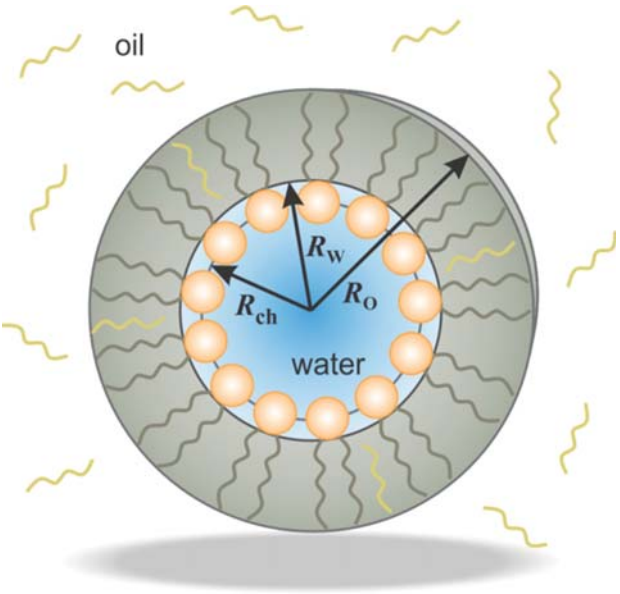

Figure 1. Schematic representation of a reverse micelle nanoparticle in a W/O microemulsion. R_W and R_O denote the size of the aqueous core and the micelle, respectively; R_{ch} designates the surface of charge.

The volume of the aggregate's interfacial layer per surfactant molecule can be related to both the volumes of the surfactant and oil molecules as well as the radii R_O and R_W via[22]

$$V_I = \frac{g_S^I v_{ST} + g_O^I v_O}{g_S^I} = v_{ST} + (g_O^I/g_S^I)v_O \tag{1a}$$

$$V_I = \frac{4\pi}{3g_S^I}(R_O{}^3 - R_W{}^3) \tag{1b}$$

where v_{ST} and v_O are the volumes of the surfactant tail and the oil molecule, respectively. As mentioned, g_S^I and g_O^I are the number of surfactant and oil molecules in the interfacial layer. The thickness of the interfacial layer is taken to be the surfactant extended tail length, l_S:

$$R_O - R_W = l_S \tag{2}$$

Combining eqs 1b and 2, one can eliminate R_O to obtain an expression for R_W in terms of V_I, g_S^I, and l_S,

$$R_W = -\frac{l_S}{2} + \frac{1}{2}\sqrt{\frac{g_S^I V_I}{\pi l_S} - \frac{1}{3}l_S{}^2} \tag{3}$$

resulting in the geometrical constraint

$$g_S^I > \frac{4\pi l_S{}^3}{3V_I} \tag{4}$$

for R_W to be positive. With R_O given by eq 2, we readily obtain the surface area of the aqueous core per surfactant molecule $a = 4\pi R_W{}^2/g_S^I$, and the total volume of the aggregate $V = 4\pi R_O{}^3/3$.

DOI: 10.1021/acs.langmuir.6b00100
Langmuir 2016, 32, 3100−3109

The above equations indicate that the geometry and size of the nanoparticle can be fully specified by two geometrical variables: (i) the number of surfactant molecules that form the droplet, g_S^I; and (ii) the ratio of oil-to-surfactant molecules in the interfacial layer, g_O^I/g_S^I. g_S^I is a convenient label for the characteristic droplet size, which can vary from the lower limit (eq 4) to an arbitrarily large value. g_O^I/g_S^I will be an independent variable in our model.

B. Gibbs Free Energy. We consider a system with a fixed composition of N_O oil molecules, N_W water molecules, and N_S amphiphile (surfactant) molecules, at temperature T and pressure p. These are the fixed parameters that characterize the mixture. The system contains a continuous oil phase with dispersed water droplets in it and may also contain an excess water phase. Both phases are allowed to contain dissolved molecules of the other components. If we consider aggregates of different sizes as distinct chemical species, the Gibbs free energy of the system at constant temperature and pressure is given by

$$G = \sum_{j,k} N_{jk}\mu_{jk} + \sum_{g_S^I} N_{g_S^I}\mu_{g_S^I} \tag{5}$$

where the subscript j = O, W, S denotes the molecule type (oil, water, surfactant) while k = O, W indicates the phase type (oil for the continuous phase, water for the excess phase). g_S^I defines the size of the micelle by indicating the number of surfactant molecules present in it. $N_{g_S^I}$ and $\mu_{g_S^I}$ are the number and chemical potential of droplets of size g_S^I, respectively. The summation over g_S^I in eq 5 accounts for the size and composition distribution (polydispersity) of the droplets.

In order to proceed, we need expressions for the various chemical potentials in eq 5. The chemical potential of component j in phase k is given by

$$\mu_{jk} = \mu_j^{ref} + kT[\ln(\gamma_{jk}X_{jk}) + U_{jk}^{hs}] \tag{6}$$

where X_{jk} is the mole fraction, γ_{jk} is the activity coefficient, μ_j^{ref} is the reference state either of the pure species or in the infinite dilution frame, depending on the component type, and U_{jk}^{hs} is a nonideality contribution due to droplet hard-sphere interactions. The expression for the chemical potential of the droplets in the continuous phase is similarly given by

$$\mu_{g_S^I} = \mu_{g_S^I}^* + kT[\ln(\gamma_{g_S^I}X_{g_S^I}) + U_{g_S^I}^{hs}] \tag{7}$$

where $\mu_{g_S^I}^*$ is the reference standard state chemical potential for a droplet of size g_S^I that is infinitely dilute in the continuous phase, $\gamma_{g_S^I}$ is the activity coefficient, $X_{g_S^I}$ is the mole fraction of droplets in the continuous phase, and $U_{g_S^I}^{hs}$ is the hard-sphere interaction. The activity coefficients appear as a result of the finite solubilities of the various components in one another, while the hard-sphere interactions are due to the presence and interactions of droplets in the continuous phase. Thus, U_{jk}^{hs} will be different from zero when k = continuous phase (droplets are present), and zero when k = excess phase (no droplets). Expressions for these terms will be given below.

The standard chemical potential $\mu_{g_S^I}^*$ of the reverse micelles can be split into two parts, one due to the interfacial layer and another due to the dispersed water domain (core) of the micelle[22]

$$\mu_{g_S^I}^* = \mu_{g_S^I}^{I*} + \sum_j g_j^{core}\mu_j^{core} \tag{8}$$

where μ_j^{core} is defined similarly to eq 6 with a hard-sphere interaction equal to zero since there are no droplets inside the droplets:

$$\mu_j^{core} = \mu_j^{ref} + kT\ln(\gamma_j^{core}X_j^{core}) \tag{9}$$

Substituting eqs 6–9 into eq 5 leads to

$$\begin{aligned} G = &\sum_{j,k} N_{jk}\mu_j^{ref} + \sum_{j,k} N_{jk}kT[\ln(\gamma_{jk}X_{jk}) + U_{jk}^{hs}] \\ &+ \sum_{g_S^I} N_{g_S^I}\mu_{g_S^I}^{I*} + \sum_j \sum_{g_S^I} N_{g_S^I}g_j^{core}\mu_j^{ref} \\ &+ \sum_j \sum_{g_S^I} N_{g_S^I}g_j^{core}kT\ln\gamma_j^{core}X_j^{core} \\ &+ \sum_{g_S^I} N_{g_S^I}kT[\ln(\gamma_{g_S^I}X_{g_S^I}) + U_{g_S^I}^{hs}] \end{aligned} \tag{10}$$

Equation 10 can be simplified by noting that the number of different kinds of molecules in each phase, N_{jk}, and the number of droplets of each size, $N_{g_S^I}$, are related to the system's total compositional parameters N_j via the following material balance equations:

$$N_j = \sum_k N_{jk} + \sum_{g_S^I} N_{g_S^I}g_j^I + \sum_{g_S^I} N_{g_S^I}g_j^{core} \tag{11}$$

Plugging eq 11 into the expression for G yields

$$\begin{aligned} G = &\sum_j N_j\mu_j^{ref} + \sum_{g_S^I} N_{g_S^I}\mu_{g_S^I}^{I*} - \sum_j \sum_{g_S^I} N_{g_S^I}g_j^I\mu_j^{ref} \\ &+ \sum_{j,k} N_{jk}kT[\ln(\gamma_{jk}X_{jk}) + U_{jk}^{hs}] \\ &+ \sum_j \sum_{g_S^I} N_{g_S^I}g_j^{core}kT\ln\gamma_j^{core}X_j^{core} \\ &+ \sum_{g_S^I} N_{g_S^I}kT[\ln(\gamma_{g_S^I}X_{g_S^I}) + U_{g_S^I}^{hs}] \end{aligned} \tag{12}$$

Since the first term in the expression depends only on the fixed system parameters N_j, we can subtract it and define G' as

$$\begin{aligned} G' = &G - \sum_j N_j\mu_j^{ref} \\ = &\{\sum_{g_S^I} N_{g_S^I}\mu_{g_S^I}^{I*} - \sum_j \sum_{g_S^I} N_{g_S^I}g_j^I\mu_j^{ref}\} \\ &+ \sum_{j,k} N_{jk}kT[\ln(\gamma_{jk}X_{jk}) + U_{jk}^{hs}] \\ &+ \sum_j \sum_{g_S^I} N_{g_S^I}g_j^{core}kT\ln\gamma_j^{core}X_j^{core} \\ &+ \sum_{g_S^I} N_{g_S^I}kT[\ln(\gamma_{g_S^I}X_{g_S^I}) + U_{g_S^I}^{hs}] \end{aligned} \tag{13}$$

where we have grouped the terms with chemical potentials inside the braces. As mentioned above, μ_j^{ref} is the reference state either of the pure species or in the infinite dilution frame, depending on the component. For oil and water molecules we use the reference state notation for the pure species ($\mu_j^{ref} = \mu_j^0$

DOI: 10.1021/acs.langmuir.6b00100
Langmuir 2016, 32, 3100–3109

for j = O, W), while for the surfactant molecules we use the notation with infinite dilution reference frame ($\mu_j^{ref} = \mu_j^*$ for j = S). We also note again that $g_W^I = 0$ as no water molecules are allowed in the micelle interfacial layer. Thus, the terms in the braces can be expanded into individual components as $\{\sum_{g_S^I} N_{g_S^I}(\mu_{g_S^I}^{I*} - g_S^I\mu_S^* - g_O^I\mu_O^0)\}$. Lastly, we divide eq 13 by kT to obtain the final dimensionless expression for the Gibbs free energy:

$$\frac{G'}{kT} = \sum_{g_S^I} N_{g_S^I} g_S^I \frac{\Delta\mu_{g_S^I}^{I*}}{kT} + \sum_{j,k} N_{jk}[\ln(\gamma_{jk}X_{jk}) + U_{jk}^{hs}] + \sum_{j,g_S^I} N_{g_S^I} g_j^{core} \ln \gamma_j^{core} X_j^{core} + \sum_{g_S^I} N_{g_S^I}[\ln(\gamma_{g_S^I} X_{g_S^I}) + U_{g_S^I}^{hs}] \quad (14)$$

where

$$\Delta\mu_{g_S^I}^{I*} = \frac{1}{g_S^I}\mu_{g_S^I}^{I*} - \mu_S^* - \frac{g_O^I}{g_S^I}\mu_O^0 \quad (15)$$

$\Delta\mu_{g_S^I}^{I*}$ is the standard free energy of micelle interface formation for a micelle of size g_S^I due to the transfer of one surfactant molecule water and g_O^I/g_S^I oil molecules from oil to the interfacial layer of the droplet. This free energy is analogous to the free energy of micelle formation in water[18] and contains several energy contributions that are discussed next.

C. Free Energy of Droplet Interface Formation $\Delta\mu_{g_S^I}^{I*}$. In the molecular thermodynamic modeling approach, the free energy change associated with the transfer of surfactant molecules from their infinitely dilute states in water and of oil molecules from the pure oil phase to the interfacial layer of the nanoparticles is expressed as the sum of several free energy contributions. This is analogous to our approach to micellization in water.[24]

$$\Delta\mu_{g_S^I}^{I*} = (\Delta\mu_{g_S^I}^{I*})_{tr} + (\Delta\mu_{g_S^I}^{I*})_{def} + (\Delta\mu_{g_S^I}^{I*})_{int} + (\Delta\mu_{g_S^I}^{I*})_{steric} + (\Delta\mu_{g_S^I}^{I*})_{ent} + (\Delta\mu_{g_S^I}^{I*})_{ionic} + (\Delta\mu_{g_S^I}^{I*})_{mix} \quad (16)$$

The energy contributions are due to (i) the transfer of surfactant tails from the solvent to the micelle; (ii) the tails' deformation in the interfacial layer; (iii) formation of an interface between the aqueous core and the nonpolar solvent; (iv) steric repulsions between surfactant headgroups at the interface; (v) mixing entropy of headgroups and counterions at the interface; (vi) ionic energy due to the assembly of all the charges (headgroups and adsorbed counterions) at the interface; (vii) a free energy due to the mixing of surfactant tails and oil molecules in the micelle interfacial layer. Similar to the treatment of micelles in water, each of these energy contributions can be computed based on the molecular structure of the various constituents and the macroscopic properties of the solution. Explicit expressions for each of the free energy contributions were presented in the earlier work on microemulsions.[23] For completeness, we provide them again in the Supporting Information.

D. Activity Coefficients. The activity coefficients describe the water and surfactant solubilities in oil, and the oil and surfactant solubilities in water. The mutual solubilities of most ternary systems are not readily available in the literature. Therefore, we use binary mutual solubilities with the assumption that the effects of the third component can be neglected. For the droplets in the continuous phase we assume that $\gamma_{g_S^I}$ is equal to 1. For the water and oil mutual solubilities, we use the UNIQUAC model for the activity coefficient. The expressions can be found in ref 28 whereas the UNIQUAC parameters for water and various alkanes are taken from ref 29.

For the activity coefficients of surfactant in the continuous oil and the excess water phase, we use the two-suffix Margules model, assuming a pseudobinary system of surfactant and water, or surfactant and oil. For the binary system, one can write

$$\ln \gamma_S = \frac{A}{RT}x_k^2 \quad (17)$$

where x_k is the mole fraction of the solvent (k = O or W), A is the parameter of the activity coefficient model, and R is the gas constant. To obtain the value of A/RT, we note that at infinite dilution

$$\gamma_S^* \equiv \lim_{x_k \to 0} \gamma_S = \exp\left(\frac{A}{RT}\right) \quad (18)$$

and, thus, $A/RT = \ln \gamma_S^*$ For the surfactant infinitely diluted in water or oil, we estimate the infinite dilution activity coefficient γ_S^* via[30]

$$\gamma_S^{*W} = (x_{CMC_W})^{-1} \quad (19a)$$

$$\gamma_S^{*O} = (x_{CMC_O})^{-1} \quad (19b)$$

E. Nonideality Due to Droplet Interactions. The hard-sphere interaction terms in eq 14 appear as a result of the mixing and interaction of droplets in the continuous phase. Since the concentration of droplets can be high, we have to take nonideal behavior into account. One approach to calculating this interaction was introduced by Overbeek,[31] who used the Percus–Yevick[32]–Carnahan–Sterling[33] equation of state for a hard-sphere suspension. The semiempirical expression has been successfully applied to explain light scattering from water droplets in organic solvents[34] and provides an expression for the osmotic pressure (or compressibility) Π of a concentrated dispersion of droplets

$$\Pi = kT\frac{\phi}{\bar{V}}\frac{1 + \phi + \phi^2 - \phi^3}{(1 - \phi)^3} \quad (20)$$

where ϕ is the volume fraction of droplets in the microemulsion and $\bar{V}$ is the average volume of a droplet. One way to think about the osmotic compressibility is that it is essentially equivalent to the compressibility of a one-component dense gas of spherical molecules. The main contribution is expected to be that of hard-sphere repulsions.[34] The relation between the osmotic pressure and the chemical potential of the various components j in the continuous oil phase (k = O) is given by[31]

$$\mu_{jO}(\phi = 0) - \mu_{jO}(\phi) = \Pi v_j \quad (21)$$

where v_j is the molecular volume of component j. Combining the two equations above, the entropic contribution due to droplet interactions becomes

$$U_{jO}^{hs} = v_j\frac{\phi}{\bar{V}}\frac{1 + \phi + \phi^2 - \phi^3}{(1 - \phi)^3} \quad (22)$$

DOI: 10.1021/acs.langmuir.6b00100
Langmuir 2016, 32, 3100–3109

To obtain the various $U^{hs}_{g^I_S}$, which are different for different droplet sizes, we assume an average value of $U^{hs}_{\bar{g}^I_S}$ for all droplet sizes that allows us to obtain the chemical potential of the hard-sphere droplets using the Gibbs–Duhem equation,

$$\sum_j X_{jO} d\mu_{jO} + d\mu_{\bar{g}^I_S} \sum_{g^I_S} X_{g^I_S} = 0 \tag{23}$$

The expression for $U^{hs}_{\bar{g}^I_S}$ is then given by[22,31]

$$U^{hs}_{\bar{g}^I_S} = \ln\left(\frac{\phi/\bar{V}}{\sum_{g^I_S} X_{g^I_S} \sum_j \phi_{jO}/v_j}\right) + \frac{\phi(7 - 3\phi - \phi^2)}{(1-\phi)^2} \tag{24}$$

F. Droplet Size Distribution (Polydispersity) and Gibbs Free Energy Minimization. The summations over g^I_S in the expression for the Gibbs free energy (eq 14) are, in theory, over all droplet sizes g^I_S. In practice, we need to reduce the infinite number of terms in eq 14 to a computationally manageable finite quantity. In our model, we perform calculations for micelle sizes up to g^I_S = 3000 surfactant molecules in the droplet interface. The number of oil molecules in the nanoparticle interfacial layer is given by the ratio of oil-to-surfactant molecules at the interface, g^I_O/g^I_S, a variable in our model. We assume that g^I_O/g^I_S is independent of micelle size. This is an assumption that reduces the number of variables from 3000 to just one. We think it is also a reasonable one, since the composition of the interface may be governed primarily by the interaction between the surfactant tails and the oil molecules as determined by their molecular structure and mutual solubility. The same line of reasoning is extended to the degree of counterion binding at the interface, β, which is also assumed to be size-independent. Together with g^I_S, these variables determine the composition, geometry, and molecular structure of each aggregate size g^I_S.

The number of droplets $N_{g^I_S}$ is different for each droplet size g^I_S. In order to reduce further the number of independent variables in eq 14 we impose a distribution on $N_{g^I_S}$ given by

$$N_{g^I_S} = N\Omega_{s\text{-}n} \tag{25}$$

where N is the total number of droplets formed in the continuous oil phase and $\Omega_{s\text{-}n}$ is a general skew-normal probability density distribution function defined by[35]

$$\Omega_{s\text{-}n}(g^I_S, \mu, \sigma, \alpha) = \frac{1}{\sigma\sqrt{2\pi}} \exp\left[-\frac{(g^I_S - \mu)^2}{2\sigma^2}\right]\left\{1 + \mathrm{erf}\left[\alpha\left(\frac{g^I_S - \mu}{\sigma\sqrt{2}}\right)\right]\right\} \tag{26}$$

with μ, σ, and α as the location, scale, and skew parameters of the distribution, respectively. μ determines the position of the distribution peak, σ describes the distribution width, and α determines the skewness, which can be positive or negative. The expression in eq 26 is very general as it can reproduce a wide range of distributions by varying the 4 independent variables N, μ, σ, and α.

Finally, we note that N_{jk} are not all independent. We choose N_{OO}, N_{WO}, and N_{SO} (the composition of the continuous oil phase) as the 3 independent variables and calculate N_{OW}, N_{WW}, and N_{SW} (the composition of the excess oil phase) using the material balance equations (eq 11) to determine the overall composition and phase behavior of the system. The global minimum of the Gibbs free energy is thus computed with respect to nine geometrically and compositionally independent variables: N_{OO}, N_{WO}, N_{SO}, N, g^I_O/g^I_S, β, μ, σ, and α.

To minimize the total Gibbs free energy, we first specify the control variables: overall composition (N_O, N_W, N_S), temperature T = 25 °C, and pressure p = 1 atm. The nine independent variables are then assigned values in a manner that is controlled by the optimization scheme used, as discussed in Results. With specified independent variables, one can readily compute the geometrical and compositional variables for the system. Then, activity coefficients, molar fractions, hard-sphere interactions, and free energies of micelle formation for each droplet size are calculated and used in the working equation, eq 14, to compute the total Gibbs free energy.

Besides the constraint on micelle size in eq 4, we impose the additional geometrical constraints that $R_{ch} > 0$ and $a > a_S$, where a is the surface area of the aqueous core per surfactant molecule and a_S is the cross-sectional area of the surfactant headgroup. There is also a geometrical constraint on the maximum packing density of droplets. Computer simulations have suggested that the maximum packing density of droplets is 0.64 in the random closed-packed limit,[36] i.e.,

$$P = \frac{N_{g^I_S\mathrm{tot}}\bar{V}}{N_{g^I_S\mathrm{tot}}\bar{V} + N_{OO}v_O + N_{SO}v_S + N_{OW}v_W} \leq 0.64 \tag{27}$$

In addition, we impose the compositional constraints that N_{jk} must be ≥0.

III. RESULTS

A. DDABr in Water and *n*-Hexane. The incorporation of micelle size distribution in the model is our most significant departure from the previous molecular thermodynamic theories on microemulsions. To determine the effect and importance of polydispersity, we first investigate the ternary mixture of didodecyl dimethylammonium bromide (DDABr), water, and *n*-hexane. This system was studied in detail by Moreira and Firoozabadi,[23] allowing us to directly compare the two approaches. Figure 2a shows a surface plot of the Gibbs free energy function versus two independent variables (a and g^I_O/g^I_S) as presented by Moreira and Firoozabadi. The other independent variables are held constant, and their values are given in ref 23. Figure 2a reveals an unusually rugged Gibbs free energy landscape with an impressive number of local minima. The authors suggest that the extreme roughness and discontinuity in the function may be due to the assumption of monodispersity which, as they point out, is quite unphysical, given the slew of experimental data that indicate that microemulsions are in fact polydisperse.[37]

We use our model to plot the Gibbs free energy in Figure 2b–d based on eq 14 and the rest of the theory, using the same surfactant molecular parameters and system compositional variables as in ref 23. Since a is not an independent variable in our model, we plot G'/kT versus g^I_O/g^I_S and three other variables: N, μ, and σ. The plots, shown in Figure 2b–d, reveal that the incorporation of polydispersity into the model has a striking effect on the landscape of the Gibbs free energy. In sharp contrast to Figure 2a, G' is now a smooth and continuous function of each of the three pairs of variables. This will affect dramatically the performance of the optimization method used for the minimization of the Gibbs free energy, as discussed next.

DOI: 10.1021/acs.langmuir.6b00100
Langmuir 2016, 32, 3100–3109

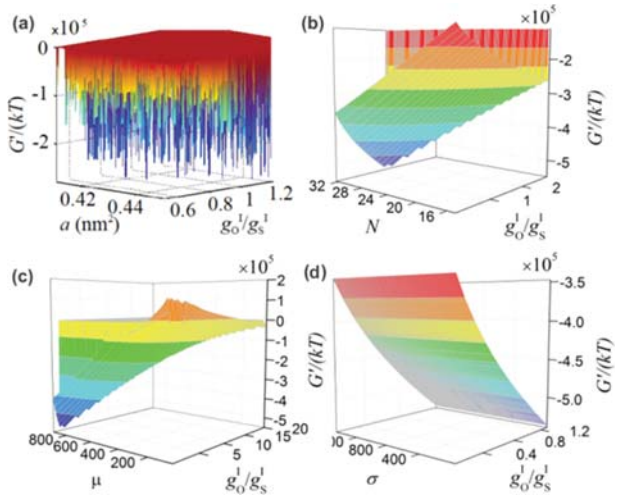

Figure 2. Surface plots showing the Gibbs free energy landscape for (a) a model without implemented polydispersity (taken from ref 23); (b–d) the model with polydispersity presented in this work. The overall composition and fixed independent variables for the system are provided in the Supporting Information and ref 23.

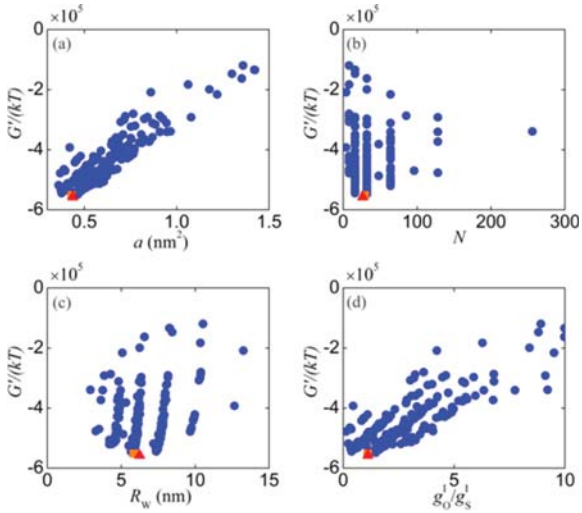

Figure 3. Minima in the total Gibbs free energy vs a, N, R_W, and g_O^I/g_S^I (a–d) for overall composition of 66/20/14 weight ratio of *n*-hexane/water/DDABr. Key: 200 PSO runs for a model without polydispersity (blue circles); 4 PSO runs for a model with polydispersity (orange squares); 1 FFSQP run for a model with polydispersity (red triangles).

To compare results for the *n*-hexane/water/DDABr system, we first seek to reproduce Moreira and Firoozabadi's data by initially removing the effect of polydispersity from our model and minimizing the Gibbs free energy with respect to the same 8 independent variables and using the same model parameters as in ref 23. Like Moreira and Firoozabadi, we use the particle swarm optimization (PSO) method to minimize G'. PSO is a heuristic optimization algorithm proposed by Kennedy and Eberhart[38] that has the advantage over direct optimization methods of being able to search the large phase space of a highly discontinuous function (as in Figure 2a) without encountering numerical difficulties. The PSO algorithm was implemented as suggested by Schwaab et al.[39] Random initial values are used for each of the independent variables, satisfying the geometrical and compositional constraints of the model. Because the PSO optimization method is stochastic, we repeat the Gibbs free energy minimization 200 times. For each PSO run, new initial estimates for the independent variables are generated using a random number generator.[23]

The results for a system with an overall composition of 66/20/14 weight ratio of *n*-hexane/water/DDABr are provided in Figure 3. The minimum values of G' for each PSO run without including polydispersity are shown in blue circles. Every blue circle corresponds to a local minimum of the Gibbs free energy, as expected from the rugged landscape seen in Figure 2a. When the 200 points are plotted on the same graph, however, a clear trend can be extrapolated toward a global minimum. Not surprisingly, the results match very well the data in ref 23 as we use the same model parameters.

More importantly, when we incorporate polydispersity, we find that the PSO method is able to locate the global minimum of the Gibbs free energy in one single run, as indicated by the orange squares in Figure 3. Each of the orange squares is in fact four distinct squares representing four independent PSO runs converging to virtually the same value for each of the four variables (Figure 3a–d). The four squares in each graph overlap and are essentially indistinguishable, suggesting that the PSO method is able to find the global minimum of G' at every run, in sharp contrast to the case without polydispersity (blue circles). While we now have the benefit of obtaining the global minimum in one PSO run, it is offset by the fact that the code with micelle size distribution is orders of magnitude slower than without it. Still, as evident from Figures 2 and 3, it appears that we now have a physically more realistic representation of the microemulsion system. One explanation for this effect can be related to metastability, as will be discussed in section IV.

The results shown in Figures 2 and 3 also suggest that we can utilize a direct optimization method such as the FFSQP algorithm[40] used in our earlier micellization model.[24] Moreira and Firoozabadi tried to implement this optimization method and encountered prohibitive numerical difficulties due to the discontinuities in G' and the inability of FFSQP to find the direction of search via its derivative methods.[23] With the incorporation of polydispersity, we encountered no such difficulties and were able to minimize the Gibbs free energy using FFSQP, resulting in faster optimization and slightly improved results compared to PSO, as indicated by the red triangles in Figure 3. Both the PSO and FFSQP optimization methods return an almost identical global minimum for the total Gibbs free energy corresponding to a droplet R_W radius of ~6 nm, which is close to the measured experimental value of 4.1 nm reported for the DDABr/water/oil system.[41] The slight discrepancy could be partially attributed to the small level of polydispersity associated with the result from the model (the size distribution is 0.8 nm wide). The effective size of the surfactant headgroup adopted by Moreira and Firoozabadi may also be imprecise, which can significantly affect the energy of droplet formation $\Delta\mu_{gs}^{I*}$ and therefore the average micelle size calculated by the model.

B. AOT in Water and Isooctane. A ternary system of significant interest is the mixture of AOT, water, and oil. AOT (dioctyl sodium sulfosuccinate) is perhaps the most widely studied surfactant known to form three-component ionic microemulsions and reverse micelles. It is of particular interest to understand how the size and morphology of AOT reverse micelles vary with the water-to-surfactant molar ratio in the

DOI: 10.1021/acs.langmuir.6b00100
Langmuir 2016, 32, 3100–3109

ternary mixture. This ratio, also known as the water loading, is defined as

$$w_0 = [H_2O]/[\text{surfactant}]$$

Two recent experimental studies have analyzed the size distribution of reverse micelles in the AOT/water/isooctane system for various water-to-surfactant ratios w_0 using dynamic light scattering (DLS)[25] and fluorescence correlation spectroscopy (FCS)[42] respectively. The results of the two investigations are replotted in Figures 4a and 4b. Reverse micelle size

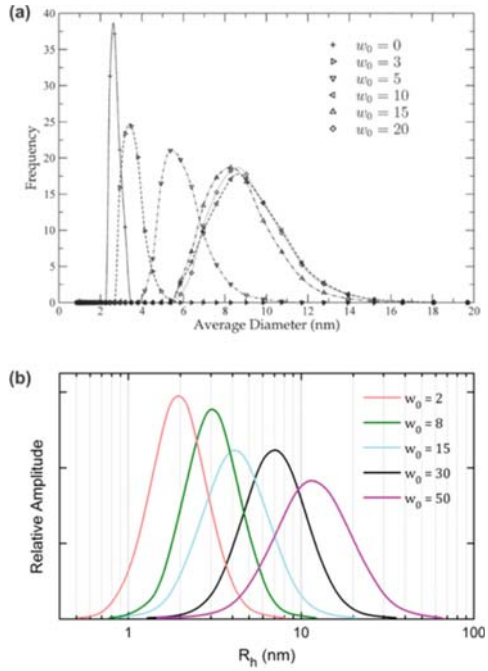

Figure 4. Reverse micelle size distributions for the AOT/water/isooctane system obtained from (a) DLS[25] and (b) FCS[42] measurements (replotted) for the water-to-surfactant ratios indicated. Details given in refs 25 and 42.

distributions from DLS measurements are plotted versus the aggregate diameters (Figure 4a), while size distributions from FCS measurements are plotted on a semilog scale versus the micelle radius (Figure 4b). Both studies reveal similar characteristics of the microemulsion system: (i) as the water loading w_0 is increased, the average micelle size increases as well; (ii) the size distributions broaden and polydispersity increases as w_0 goes up; (iii) the size distributions are asymmetric (positively skewed) and span a range of several nanometers even at low values of w_0; (iv) the peaks become smaller with increasing w_0 due to the broadening of the distributions.

We model the AOT/water/isooctane system for different values of w_0 using the system composition ratios provided in ref 25. We adopt a value of 50 Å^2 for the cross-sectional area of the surfactant headgroup[43,44] and CMC values of 0.5 mM and 2.5 mM for AOT in isooctane and water, respectively.[44,45] Other surfactant and solvent structural parameters relevant to the calculation of the activity coefficients and the free energy of micelle formation are listed in the Supporting Information. In light of the results in the previous section, we opted for the FFSQP method to optimize G' for the AOT/water/isooctane system. We should note that the results for this system were somewhat dependent on initial conditions. A more robust and up-to-date optimization method may perform more reliably than the FFSQP.

The calculated size distribution functions are shown in Figure 5. As evident from the plot, the experimental trends are

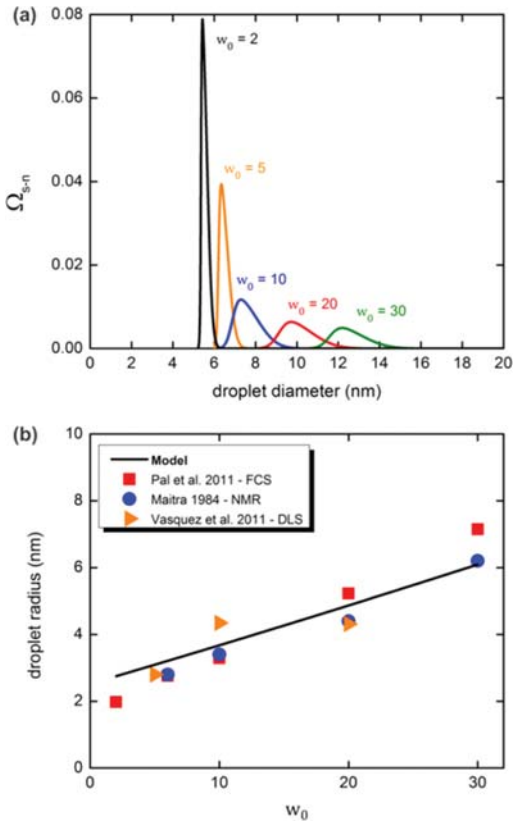

Figure 5. (a) Model predictions for the droplet size distributions in the AOT/water/isooctane system at the water-to-surfactant ratios indicated. (b) Calculated and experimental[25,42,46] variation of the average micelle size as a function of w_0 for the AOT/water/isooctane system. A list of the compositional and geometrical parameters for a sample run (w_0 = 10) is provided in the Supporting Information.

reasonably well reproduced. In agreement with Figure 4, we observe asymmetric and positively skewed size distributions that become broader and shift to larger droplet sizes as the water loading w_0 is increased. We should emphasize again that all distribution parameters (peak location, width, and skewness) are independent variables in the model and are thus solely determined by the optimization algorithm and the location of the global minimum of the Gibbs free energy. We also notice that differences in the distribution peak amplitudes are more pronounced in the model. Nevertheless, the overall trends are captured well.

Besides reasonable agreement with experiment in terms of trends, we also observe good quantitative agreement in terms of the values for the average droplet sizes as a function of w_0. This is shown in Figure 5b, where we plot the calculated dependence of the average droplet size on w_0 and compare it to experimental values, including a nuclear magnetic resonance (NMR) study of the AOT/water/isooctane system.[46] The NMR data may be more reliable since light scattering measurements are less dependable near the optical matching point of the microemulsion droplets ($w_0 \approx 25$).[42] We notice

DOI: 10.1021/acs.langmuir.6b00100
Langmuir 2016, 32, 3100−3109

that the model predicts accurately the micelle size variation with w_0 and is a reasonably good fit for each of the three experimental studies. It is generally assumed that reverse micelle sizes vary linearly with w_0, and the fact that we observe a linear dependence is encouraging.

Along with specifics about the micelle sizes and size distributions, the model provides details about the overall phase behavior, as well as the finer molecular structure of the nanoparticles. The former is illustrated in Figure 6a where we plot the total number of droplets formed in the continuous oil phase, as well as the fraction of water in the dispersed and excess water phases. As water is added to the system, the micelles begin to grow in size whereas the total number of droplets in the system starts to decrease. At low water loading ($w_0 < 5$) there is no excess water phase and virtually all water molecules reside within the dispersed phase contained in the micelles' aqueous cores. As more water is added, the droplets cannot accommodate all water molecules and a small excess water phase starts to form.

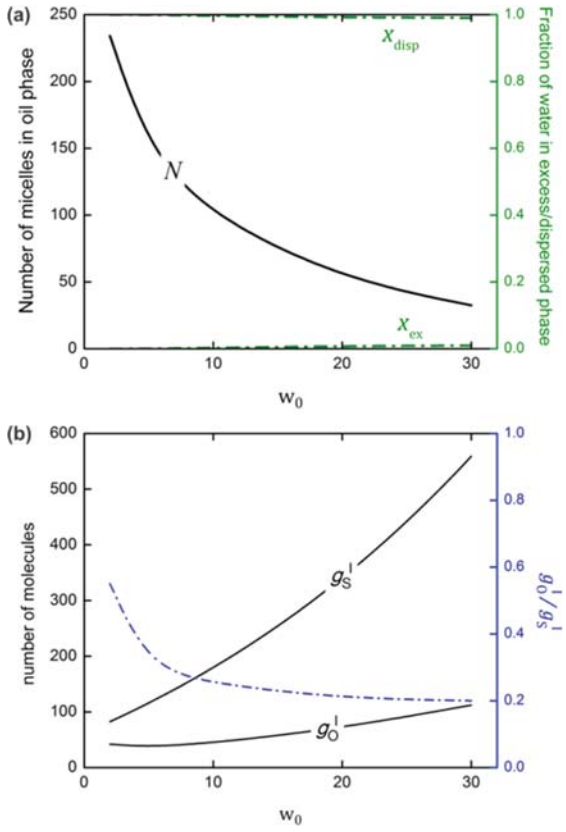

Figure 6. (a) Phase behavior: total number of droplets in the continuous phase and size of excess phase. (b) Molecular structure of the reverse micelles at peak size as a function of w_0: number of surfactant and oil molecules in the micelle interface (black); ratio of oil-to-surfactant molecules in the interface (blue).

Details of the nanoparticles' molecular structure are shown in Figure 6b, where we plot the average number of surfactant and oil molecules in the droplets' interface as a function of w_0. As one might expect, the number of surfactant molecules in the micelle interface increases with droplet size and so does the number of oil molecules. The ratio of oil-to-surfactant molecules g_O^I/g_S^I remains relatively constant with water loading for $w_0 > 5$. For $w_0 < 5$, however, it starts to increase as the average droplet size becomes smaller.

IV. DISCUSSION

The fact that the ratio of oil-to-surfactant molecules increases for $w_0 < 5$ suggests that our assumption of constant g_O^I/g_S^I for different micelle sizes begins to break down at very low w_0. This makes physical sense: as the droplets become increasingly small, their curvature increases dramatically and more space opens up for oil molecules to be accommodated among the surfactant tails in the interfacial layer. This also means that the model becomes increasingly inaccurate at very low water loading. For $w_0 < 2$ we encounter another limitation: as the surfactant heads become more tightly packed inside the droplets, we approach the constraint boundary $a > a_S$, where a is the surface area of the aqueous core per surfactant molecule and a_S is the cross-sectional area of the surfactant headgroup. As a result, the optimization routine starts to experience numerical difficulties in searching for a minimum that is very close to the phase-space boundary.

One assumption in our model is that no oil or surfactant molecules remain dissolved in the aqueous cores of the droplets. While this assumption is certainly reasonable for oil molecules, which have very low solubility in water, it may be inaccurate for certain surfactants that are more soluble in water. To allow for the possibility that some surfactant molecules are dissolved in the aqueous cores, especially for larger-size droplets, we ran the model with one additional independent variable: the ratio of surfactant-to-water molecules in the core g_S^{core}/g_W^{core}. We obtained identical results, with an average number of 0.1 surfactant molecule per aqueous core for the largest water content we tested ($w_0 = 30$), and much less than that for lower w_0, suggesting that surfactant monomer presence in the aqueous cores can be neglected without loss of accuracy.

An important question to address is why a monodisperse model produces such a rugged Gibbs energy surface compared to a model with polydispersity (Figure 2). One explanation can be related to metastability.[47] When we artificially impose one droplet size (i.e., monodispersity) on a system that is polydisperse by nature, a very large number of metastable states (local minima) arise. Collectively, these states correspond to the continuum of droplet sizes that are in fact physically present in the system. As the artificial constraint of monodispersity is removed and a distribution of sizes is allowed in the formulation, the various droplet sizes become accounted for through this distribution and the metastable states no longer appear. This can be seen quantitatively in Figure 3, where we plot the minima of the Gibbs free energy for all PSO runs vs one variable at a time. The large number of minima in the monodisperse system (blue circles) trace out a distribution of values for each variable. For the polydisperse system the Gibbs energy minimum is only one (orange squares and red triangle corresponding to the global minimum) with the distribution now represented through the three independent variables σ, μ, and α.

While we do impose a skew normal probability distribution on the system externally through eq 26, the equation is very general and allows for distributions of various widths, peak locations, and skewness to be selected by the optimization routine by varying the independent variables σ, μ, and α. The distribution ultimately selected corresponds to the lowest Gibbs free energy that the optimization method is able to find. This is largely determined by the energy of droplet formation $\Delta\mu_{g_S^I}^{I*}$

DOI: 10.1021/acs.langmuir.6b00100
Langmuir 2016, 32, 3100−3109

(and its constituent energy contributions) for each droplet size g_S^I. As a result, eq 26 is simply a convenient tool that allows for the underlying physics of the problem to be accessed.

V. CONCLUSIONS

We have developed a molecular thermodynamic theory for polydisperse reverse micelles and W/O microemulsions that allows for the prediction of nanoparticle sizes and size distributions based on global minimization of the Gibbs free energy. The expression for the Gibbs free energy is used together with the free energy of micelle formation, which accounts for various contributions related to the formation of the droplet interfacial layer as well as to the surfactant and solvent molecular structure. The incorporation of polydispersity in the model improves the landscape of the Gibbs free energy function and allows for more efficient and more reliable access to the global minimum. We use no fitted or adjustable parameters. To test the model, we analyzed two different ternary systems composed of DDABr/water/*n*-hexane and AOT/water/isooctane. We find that the model captures well the structure and behavior of the former, and the average droplet sizes and size distributions as a function of the water-to-surfactant ratio in the latter. The ability to provide details about the phase behavior and the nanoparticles' molecular structure, and thus bridge the gap between the macroscopic and the microscopic worlds, is one of the key features of the molecular thermodynamic approach. The potential practical implications lie in the ability to predict the phase behavior and molecular structure of systems that may not be experimentally accessible, or to help alleviate the need for costly and time-consuming trial-and-error type experiments. This attribute of the model can be useful in studies concerned with the self-assembly of amphiphilic molecules such as the formation of phospholipid membranes[48] or the development of artificial cellular systems.

■ ASSOCIATED CONTENT

Supporting Information

The Supporting Information is available free of charge on the ACS Publications website at DOI: 10.1021/acs.langmuir.6b00100.

Molecular and compositional parameters and expressions for free energy contributions to the energy of interface formation (PDF)

■ AUTHOR INFORMATION

Corresponding Author

*E-mail: abbas.firoozabadi@yale.edu.

Notes

The authors declare no competing financial interest.

■ ACKNOWLEDGMENTS

The authors thank the member companies of the Reservoir Engineering Research Institute (RERI) in Palo Alto, CA, for the financial support, and their colleagues at RERI for many helpful discussions.

■ REFERENCES

(1) Fanun, M. *Microemulsions: Properties and Applications*; CRC Press: Boca Raton, FL, 2009.

(2) Liz-Marzan, L. M.; Kamat, P. V. Synthesis of Nanoparticles in Microemulsions. In *Nanoscale Materials*; Kluwer Academic Publishers: Dordrecht, 2003; pp 135−155.

(3) Zhang, S.; Zhao, Y. Facile Preparation of Organic Nanoparticles by Interfacial Cross-Linking of Reverse Micelles and Template Synthesis of Subnanometer Au-Pt Nanoparticles. *ACS Nano* **2011**, *5*, 2637−2646.

(4) Lawrence, M. J.; Rees, G. D. Microemulsion-based media as novel drug delivery systems. *Adv. Drug Delivery Rev.* **2000**, *45*, 89−121.

(5) Trivedi, R.; Kompella, U. B. Nanomicellar formulations for sustained drug delivery: strategies and underlying principles. *Nanomedicine* **2010**, *5*, 485−505.

(6) Shah, D. O. *Surface Phenomena in Enhanced Recovery*; Plenum Press: New York, NY, 1981.

(7) Van Horn, W. D.; Ogilvie, M. E.; Flynn, P. F. Reverse Micelle Encapsulation as a Model for Intracellular Crowding. *J. Am. Chem. Soc.* **2009**, *131*, 8030−8039.

(8) Maruyama, T.; Park, L.-C.; Shinohara, T.; Goto, M. DNA Hybridization in Nanostructural Molecular Assemblies Enables Detection of Gene Mutations without a Fluorescent Probe. *Biomacromolecules* **2004**, *5*, 49−53.

(9) Zhou, J.; Wei, C.; Jia, G.; Wang, X.; Feng, Z.; Li, C. Formation and stabilization of G-quadruplex in nanosized water pools. *Chem. Commun.* **2010**, *46*, 1700−1702.

(10) Van Horn, W. D.; Simorellis, A. K.; Flynn, P. F. *J.* Low-Temperature Studies of Encapsulated Proteins. *J. Am. Chem. Soc.* **2005**, *127*, 13553−13560.

(11) Simorellis, A. K.; Van Horn, W. D.; Flynn, P. F. Dynamics of Low Temperature Induced Water Shedding from AOT Reverse Micelles. *J. Am. Chem. Soc.* **2006**, *128*, 5082−5090.

(12) Adamson, A. W. A model for micellar emulsions. *J. Colloid Interface Sci.* **1969**, *29*, 261−267.

(13) Friberg, S.; Mandell, L.; Larsson, M. Mesomorphous phases, a factor of importance for the properties of emulsions. *J. Colloid Interface Sci.* **1969**, *29*, 155−156.

(14) Ruckenstein, E.; Nagarajan, R. Aggregation of amphiphiles in nonaqueous media. *J. Phys. Chem.* **1980**, *84*, 1349−1358.

(15) Khoshnood, A.; Firoozabadi, A. Polar Solvents Trigger Formation of Reverse Micelles. *Langmuir* **2015**, *31*, 5982−5991.

(16) Overbeek, J. T. G.; Verhoeckx, G. J.; de Bruyn, P. L.; Lekkerkerker, H. N. W. On Understanding Microemulsions. II. Thermodynamics of Droplet-Type Microemulsions. *J. Colloid Interface Sci.* **1987**, *119*, 422−441.

(17) Lam, A. C.; Falk, N. A.; Schechter, R. S. The Thermodynamics of Microemulsions. *J. Colloid Interface Sci.* **1987**, *120*, 30−41.

(18) Ruckenstein, E. Thermodynamics of Microemulsions: Relation Between Their Structure and Phase Behavior. *Fluid Phase Equilib.* **1985**, *20*, 189−206.

(19) Peck, D. G.; Schechter, R. S.; Johnston, K. P. Unified Classical and Molecular Thermodynamic Theory of Spherical Water-in-Oil Microemulsions. *J. Phys. Chem.* **1991**, *95*, 9541−9549.

(20) Borkovec, M. Phenomenological Theories of Globular Microemulsions. *Adv. Colloid Interface Sci.* **1992**, *37*, 195−217.

(21) Bergström, L. M. Influence of bending energetics on the size, shape and polydispersity of droplet microemulsions. *Colloids Surf., A* **2008**, *316*, 15−26.

(22) Nagarajan, R.; Ruckenstein, E. Molecular Theory of Microemulsions. *Langmuir* **2000**, *16*, 6400−6415.

(23) Moreira, L. A.; Firoozabadi, A. Molecualr Thermodynamic Modeling of Droplet-Type Microemulsions. *Langmuir* **2012**, *28*, 1738−1752.

(24) Lukanov, B.; Firoozabadi, A. Specific Ion Effects on the Self-Assembly of Ionic Surfactants: A Molecular Thermodynamic Theory of Micellization with Dispersion Forces. *Langmuir* **2014**, *30*, 6373−6383.

(25) Vasquez, V. R.; Williams, B. C.; Graeve, O. A. Stability and Comparative Analysis of AOT/Water/Isooctane Reverse Micelle System Using Dynamic Light Scattering and Molecular Dynamics. *J. Phys. Chem. B* **2011**, *115*, 2979−2987.

(26) Chowdhary, J.; Ladanyi, B. M. Molecular Dynamics Simulation of Aerosol-OT Reverse Micelles. *J. Phys. Chem. B* **2009**, *113*, 15029−15039.

DOI: 10.1021/acs.langmuir.6b00100
Langmuir 2016, 32, 3100−3109

(27) Abel, S.; Sterpone, F.; Bandyopadhyay, S.; Marchi, M. Molecular Modeling and Simulations of AOT-Water Reverse Micelles in Isooctane: Structural and Dynamic Properties. *J. Phys. Chem. B* **2004**, *108*, 19458−19466.
(28) Poling, B. E.; Prausnitz, J. M.; Connell, J. O. *The Properties of Gases and Liquids*, 5th ed.; McGraw-Hill: New York, 2000.
(29) Sorensen, J. M.; Arlt, W. *Liquid-Liquid Equilibrium Data Collection. 1, Binary Systems: Tables, Diagrams, and Model Parameters*; DECHEMA: Frankfurt/Main, Germany, 1979.
(30) Viades-Trejo, J.; Amigo, A.; Gracia-Fadrique, J. Activity coefficients at infinite dilution for surfactants. *Fluid Phase Equilib.* **2006**, *250*, 158−164.
(31) Overbeek, J. T. G. The First Rideal Lecture. Microemulsions, a field at the border between lyophobic and lyophilic colloids. *Faraday Discuss. Chem. Soc.* **1978**, *65*, 7−19.
(32) Percus, J. K.; Yevick, G. J. Analysis of Classical Statistical Mechanics by Means of Collective Coordinates. *Phys. Rev.* **1958**, *110*, 1−13.
(33) Carnahan, N. F.; Starling, K. E. Equation of State for Nonattracting Rigid Spheres. *J. Chem. Phys.* **1969**, *51*, 635−636.
(34) Agterof, W. G. M.; van Zomeren, J. A. J.; Vrij, A. On the application of hard sphere fluid theory to liquid particle dispersions. *Chem. Phys. Lett.* **1976**, *43*, 363−367.
(35) O'Hagan, A.; Leonard, T. Bayes estimation subject to uncertainty about parameter constraints. *Biometrika* **1976**, *63*, 201−203.
(36) Farr, R. S.; Groot, R. D. Close packing density of polydisperse hard spheres. *J. Chem. Phys.* **2009**, *131*, 244104.
(37) Eriksson, J. C.; Ljunggren, S. Thermodynamic Evaluation of the Polydispersity of Droplet Microemulsions. *Langmuir* **1995**, *11*, 1145−1153.
(38) Kennedy, J.; Eberhart, R. Particle Swarm Optimization. *Proc. IEEE Int. Conf. Neural Networks* **1995**, *4*, 1942−1948.
(39) Schwaab, M.; Biscaia, E. C., Jr.; Monteiro, J. L.; Pinto, J. C. Nonlinear parameter estimation through particle swarm optimization. *Chem. Eng. Sci.* **2008**, *63*, 1542−1552.
(40) Zhou, J. L.; Tits, A. L.; Lawrence, C. T. *User's Guide for FFSQP Version 3.7: A FORTRAN Code for Solfing Constrained Nonlinear (Minimax) Optimization Problems, Generating Iterates Satisfying All Inequality and Linear Constraints*; Electrical Engineering Dept and Institute for Systems Research, University of Maryland: College Park, MD, 1997.
(41) Chen, S. J.; Evans, D. F.; Ninham, B. W.; Mitchell, D. J.; Blum, F. D.; Pickup, S. Curvature as a determinant of microstructure and microemulsions. *J. Phys. Chem.* **1986**, *90*, 842−847.
(42) Pal, N.; Verma, S. D.; Singh, M. K.; Sen, S. Fluorescence Correlation Spectroscopy: An Efficient Tool for Measuring Size, Size-Distribution and Polydispersity of Microemulsion Droplets in Solution. *Anal. Chem.* **2011**, *83*, 7736−7744.
(43) Hellsing, M. S.; Rennie, A. R. Effect of Concentration and Addition of Ions on the Adsorption of Aerosol-OT to Sapphire. *Langmuir* **2010**, *26*, 14567−14573.
(44) Zulauf, M.; Eicke, H.-F. Inverted micelles and microemulsions in the ternary system water/aerosol-OT/isooctane as studied by photon correlation spectroscopy. *J. Phys. Chem.* **1979**, *83*, 480−486.
(45) Li, Z. X.; Lu, J. R.; Thomas, R. K.; Penfold, J. Neutron Reflectivity Studies of the Adsorption of Aerosol-OT at the Air-Water Interface: The Structure of the Sodium Salt. *J. Phys. Chem. B* **1997**, *101*, 1615−1620.
(46) Maitra, A. Determination of size parameters of water-Aerosol OT -oil reverse micelles from their nuclear magnetic resonance data. *J. Phys. Chem.* **1984**, *88*, 5122−5125.
(47) Firoozabadi, A. *Thermodynamics and Applications of Hydrocarbons Energy Production*; McGraw-Hill: New York, NY, 2015.
(48) Budin, I.; Devaraj, N. K. Membrane Assembly Driven by a Biomimetic Coupling Reaction. *J. Am. Chem. Soc.* **2012**, *134*, 751−753.

DOI: 10.1021/acs.langmuir.6b00100
Langmuir 2016, 32, 3100−3109